PHYSICAL REVIEW B **83**, 035416 (2011)

Photon mapping of individual Ag particles on MgO/Mo(001)

Philipp Myrach, Niklas Nilius,* and Hans-Joachim Freund

Fritz-Haber Institut der Max-Planck Gesellschaft, Department of Chemical Physics, Faradayweg 4-6, D-14195 Berlin, Germany

(Received 15 October 2010; revised manuscript received 9 November 2010; published 20 January 2011)

The optical properties of single Ag particles on an MgO thin film have been investigated with fluorescence spectroscopy performed in a scanning-tunneling-microscope setup. Depending on the point of excitation within the particle (top or side facet), two emission maxima are detected that are compatible with the in-plane and out-of-plane plasmons of the Ag deposits. The different excitation cross sections and spectral properties of the two modes give rise to characteristic intensity patterns in photon maps taken from individual particles.

DOI: 10.1103/PhysRevB.83.035416 PACS number(s): 78.67.Hc, 68.47.Jn, 68.37.Ef

I. INTRODUCTION

Classical wave optics sets a natural limit to the spatial resolution of far-field optical microscopy. According to the Abbes diffraction limit,[1] two pointlike photon sources can only be distinguished if their mutual distance is larger than half the wavelength of the emitted radiation divided by the refractive index of the environment. The achievable resolution is therefore of the order of 250 nm ($\lambda_{rad} \sim 500$ nm), hence much larger than the size of nano-objects, for example, molecules, quantum dots, or metal particles.

Virtually since its formulation in the 19th century, scientists have tried to override this resolution limit by introducing new, sophisticated optical techniques. Confocal fluorescence microscopy[2] and different pulsed optical methods[3] turned out to be promising far-field approaches; however, near-field techniques also demonstrated their ability to achieve subwavelength spatial resolution. In the latter case, either the excitation or the detection of the optical signal is realized by a sensor placed in nanometer distance from the surface. Scanning near-field optical microscopy is used for a local optical excitation of the sample,[4] while scanning tunneling microscopy enables an electronic stimulation followed by photon detection in the far field.[5,6] The scanning tunneling microscopy approach is capable of measuring the emission response of nanometer-sized regions, as the diameter of the exciting electron beam and not the nature of light propagation sets the resolution limit. The method has been successfully employed to probe the optical properties of individual metal clusters,[7,8] semiconductor quantum dots,[9,10] and organic molecules.[11,12] In addition to the optical measurement, the surface morphology can be simultaneously probed by the scanning-tunneling-microscope (STM) tip. This combination, commonly known as photon mapping, provides information on the nature of the individual emission centers on the surface.[10,13–15]

In this study, we exploit the capabilities of the STM to explore the emission properties of individual metal nanoparticles deposited on an oxide support. Such cluster-oxide systems are of crucial importance for photocatalytic and photovoltaic applications, for example, in solar cells.[16] Here the particles act as nanoantennas, storing the incoming radiation in the form of collective electronic excitations with high oscillator strength (plasmons). The plasmons are then converted into electron-hole pairs (excitons) that finally induce the photon-mediated reaction. To optimize the interplay between plasmonic and excitonic modes, the influence of the particle geometry on the optical properties needs to be determined. These data are hard to obtain with nonlocal optical techniques due to the inherent size and shape distribution of particles in an ensemble.[17] However, averaging effects can be avoided with STM fluorescence spectroscopy, which addresses each particle individually. The strength of this method has already been demonstrated in various experiments that examined the role of chemical identity,[15,18] size and shape,[8] and support material[19] on the emission properties of metal aggregates. In this study, we report on spatially resolved measurements performed on single Ag particles grown on an MgO/Mo(001) film. The experiments identify regions of the particles, where mainly the in-plane (1,1) and the out-of-plane (1,0) plasmon can be stimulated with the electron beam.

II. EXPERIMENT

The experiments are performed with a liquid-nitrogen-cooled STM operated in ultrahigh vacuum (2×10^{-10} mbar). The beetle-type STM head is surrounded by a parabolic mirror of 40 mm diameter that collects photons emitted from the tip-sample junction. A second mirror outside the vacuum chamber focuses the light either into the entrance slit of a grating spectrograph coupled to a charge-coupled device detector or into a photomultiplier tube. While the first option is used to record emission spectra in a wavelength window between 200 and 1000 nm, the second one enables the acquisition of maps of the integral photon intensity. The tip is made from an Ag wire, electrochemically etched under the control of a light microscope.

The MgO films used as particle support are prepared by Mg deposition in 5×10^{-7} mbar O_2 at 300 K onto a sputtered and flashed Mo(001) surface.[20] After deposition, the films are annealed to 1100 K in order to improve their crystallinity. For an MgO thickness of 10–12 Monolayer (ML) as used here the oxide surface exhibits a network of misfit dislocations running along the nonpolar ⟨100⟩ directions [Fig. 1(a)]. In addition, a faint square pattern that marks the interfacial MgO-Mo coincidence lattice of 55×55 Å^2 size is discernable. Both the dislocation lines and the coincidence lattice are introduced to compensate the 5.4% lattice mismatch between oxide film and metal support.[20] Silver atoms are deposited onto the freshly prepared oxide surface at 300 K from a Mo crucible heated by electron bombardment (flux 0.25 ML/min).

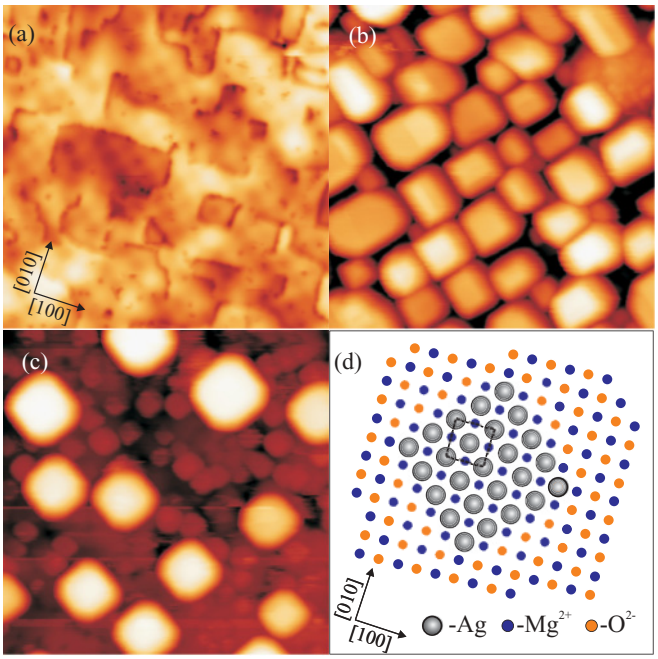

FIG. 1. (Color online) STM topographic images of (a) the bare 10-ML-thick MgO/Mo(001) film, (b) after deposition of nominally 2 ML Ag at 300 K ($U_s = 3.0$ V, 75×75 nm^2), and (c) after annealing to 500 K ($U_s = 6.0$ V, 50×50 nm^2). (d) Structure model of the Ag-MgO interface as deduced from the shape and orientation of the Ag deposits.

III. RESULTS AND DISCUSSIONS

A. Morphology of the Ag particles

Figure 1(b) shows an STM image of the resulting particle ensemble on the MgO film. Silver nucleates into three-dimensional (3D) deposits with distinct square and rectangular shapes. Their aspect ratio (height/diameter) amounts to ~0.7, which has to be taken as lower bound due to tip convolution effects. The twofold symmetry of Ag deposits indicates good interfacial registry with the MgO surface. The Ag atoms are expected to bind on top of the lattice oxygen,[21] a geometry that is compatible with the 3% lattice mismatch between Ag(001) and MgO(001). The Ag⟨110⟩ direction hereby aligns with MgO⟨110⟩ (the direction of the O rows), defining the orientation of the particle edges [Fig. 1(d)]. The well-behaved growth of Ag on MgO(001) does not come as a surprise, as Ag(001) in turn is a widely used substrate to prepare atomically flat MgO films.[22] The density of Ag particles upon room temperature deposition amounts to 1×10^{12} cm^{-2}, whereby the MgO dislocation network provides the relevant nucleation sites. Distinct changes in the particle morphology occur after annealing the sample to 500 K [Fig. 1(c)]. While the cluster density declines by roughly a factor of 3 (3×10^{11} cm^{-2}) due to efficient ripening processes at the surface, the particles become larger and their aspect ratio approaches 1. The pronounced vertical growth of Ag on MgO(001) reflects the small interfacial adhesion between both materials, being related to the low heat of oxidation of silver.[21,23] A twofold symmetric basal plane together with a large height results in the development of nearly cubic silver deposits with up to 10-nm side length. This particular shape is further promoted by the fact that all side facets comprise stable Ag(100) planes.

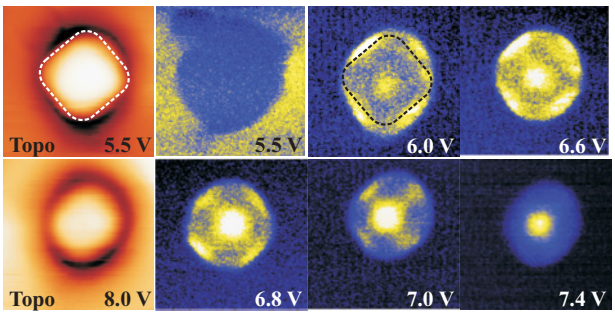

FIG. 2. (Color online) STM topographic images and photon maps of an Ag particle on MgO/Mo(001) taken as a function of sample bias ($I = 1$ nA, 8×8 nm^2). The apparent cluster height continuously decreases with bias voltages. The light emission starts at the four side facets of the particle and localizes on the top facet at higher bias.

B. Optical properties of the Ag particles

Light-emission data are exclusively obtained from annealed samples in order to minimize the effect of particle-particle interactions on the optical response. First, photon maps of selected Ag deposits are taken; the hereby identified regions of high emission yield are later used to acquire the spectral data. Figure 2 displays photon maps of a typical Ag particle of ~4 nm diameter taken as a function of the excitation bias. At low bias (5–6 V), only the MgO substrate emits light. The underlying mechanism has been identified before as radiative electron transitions between vacuum states in front of the surface (field-emission resonances) and the MgO conduction band.[24] Light emission from the cluster sets in only above 6.0 V. Surprisingly, not the center of the nanocube, but the four side facets start to emit photons. With increasing bias, the central part of the deposit becomes brighter until it dominates the photon maps above 7.0 V. At even higher bias, the emission intensity declines again, whereby the particle center remains optically active until ~9.0 V. The four corners of the cube do not contribute to the optical signal at all relevant excitation conditions.

To understand the spatial distribution of the emission, we have performed photon spectroscopy on a similar cluster. The first set of spectra is taken at low excitation bias, where mainly the side facets determine the optical response [$U_s = +6.5$ V, Fig. 3(a)] As expected, the overall intensity is larger when the tip is placed above one of the four edges compared to the particle center. The spectral course is governed by three emission bands. The dominant one is centered at around 600 nm (2.1 eV) and has a full width at half maximum (FWHM) of 0.5 eV. It displays a fine structure, consisting of five equally spaced maxima, the origin of which is not fully understood at this point.[25] The other bands at 450 nm (2.75 eV, FWHM 0.6 eV) and 760 nm (1.65 eV, FWHM 0.2 eV) are exclusively observed in spectra taken above the particle edges. The spectral response from the side facets vanishes at higher excitation bias (7.9 V), while a signal remains detectable in the center. This behavior mimics the intensity distribution observed in the respective photon maps [Fig. 3(b), inset].

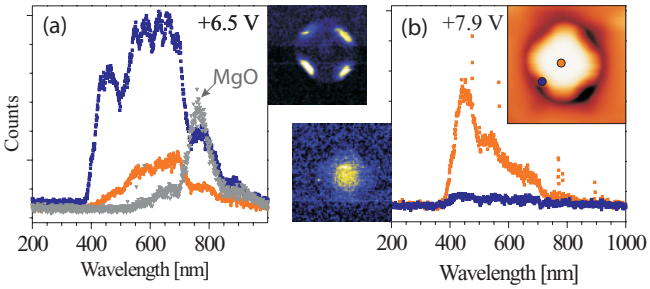

FIG. 3. (Color online) Light-emission spectra taken at the side (dark blue) and top facet (light orange) of a single Ag particle at (a) 6.5 V and (b) 7.9 V as well as on the bare MgO surface (grey). The tip positions for spectroscopy are marked in the right inset (7×7 nm^2). The emission intensity is higher at the particle edges at low excitation bias, but moves to the center at higher bias. Similar behavior is observed in the photon maps of the same deposit (insets in the middle).

Spectroscopically the photon peak at 2.75 eV gains intensity with respect to the 2.1-eV emission band, while the 1.65-eV peak disappears at high excitation voltage. A similar emission behavior was revealed for other particles in this study with only the maximum positions slightly varying from case to case.

C. Discussion

The emission response of Ag particles in the STM junction can only be understood in the framework of plasmonic excitations, which are particularly strong for noble metal clusters.[17] The plasmons are stimulated by electron injection from the STM tip and decay to some extent radiatively. The emission probability hereby depends on dielectric losses in the cluster, rendering silver the ideal material due to the low imaginary part of its dielectric function below the *d*-band onset. Two dipolar plasmon modes are expected for cube-shaped particles, an out-of-plane (1,0) mode oscillating perpendicular to the surface, and a degenerate in-plane (1,1) mode.[17,26] The modes have different energies, as the polarizable MgO/Mo support breaks the symmetry of the electromagnetic excitation. For spherical (instead of cubic) Ag clusters on bulk MgO, the plasmon energies can be calculated with the GRANFILM program developed by Lazzari and Simonsen.[27] The code determines the particle polarizability by solving the Maxwell equations in a quasistatic regime. Hereby, measured particle sizes/shapes are used to reproduce the experimental situation, while the material constants for Ag and MgO are taken from the literature.[28] A calculated absorption spectrum for a 4-nm Ag sphere is shown in Fig. 4(a). It clearly displays the double-peak structure due to in-plane (455 nm or 2.7 eV) and out-of-plane plasmon excitations (365 nm or 3.4 eV).

So far, the location of the Ag particle in the tip-sample contact of an STM has been neglected. However, it is well known that the emission from an ideal dipole source is altered by the strong near field in the tip-sample junction.[6,29] In fact, only this field enhancement renders optical spectroscopy of individual nano-objects feasible in the STM. For the Ag tip–Mo sample junction used here, the enhancement window stretches from approximately 1.5 to 3.7 eV, defining the spectral region in which plasmon-mediated light emission can

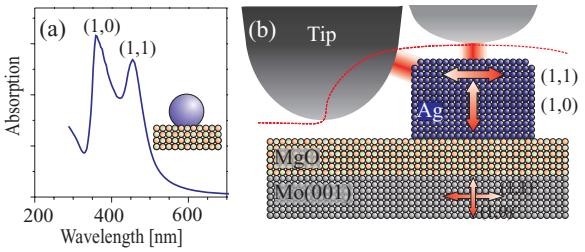

FIG. 4. (Color online) (a) Calculated absorption spectrum of a spherical Ag particle of 4 nm diameter on MgO(001). (b) Sketch of the tip-sample geometry for exciting the in-plane (1,1) and out-of-plane (1,0) plasmons (big arrows). Image dipoles in the support are depicted by smaller arrows. The dashed line marks the trajectory of the tip when moving across the particle.

be detected.[29] In addition, the cavity acts as a polarizable environment for the metal particle, which induces a considerable redshift of its plasmon modes. A similar behavior is observed for metal particles embedded in a dielectric matrix that enhances the particle polarizabiltiy and lowers its plasmon energy.[17]

Based on these considerations, the three emission bands observed in Fig. 3(a) can be assigned. The low-energy peak at 1.65 eV that does not only appear on the cluster edges but also on the bare MgO relates to radiative electron transitions via field-emission resonances in front of the surface, as discussed before.[24] The other two bands are assigned to the in-plane (2.1 eV) and out-of-plane Ag plasmon modes (2.75 eV), implying a downshift of $\sim$0.6 eV with respect to their calculated positions. Such a shift is compatible with the anticipated influence of the STM tip on the cluster polarizability.[29] The visibility of the two modes on either top or side facet of the particle can be related to different excitation geometries. Above the edge, the tip electrons are injected almost horizontally into the deposit and carry a large in-plane dipole moment that couples to the (1,1) plasmon [Fig. 4(b), left]. Consequently, this mode appears in the photon maps as emission pockets located at the four side facets of the particle. If the tip moves toward the center, the direction of the electron beam becomes more vertical and the horizontal mode vanishes [Fig. 4(b), right]. The same effect occurs at higher excitation bias, as the associated increase in the tip-sample distance also enlarges the inclination of the electron beam against the surface. The out-of-plane plasmon, on the other hand, is best visible above the particle center, when the tip electrons transfer a large dipole moment in the vertical direction.

The visibility of horizontal plasmon modes is surprising, as the specific tip-sample geometry in an STM enhances mainly the emission from vertical dipole sources. In fact, in-plane modes induce image dipoles with opposite orientation in both tip and sample, which tend to quench the original excitation [Fig. 4(b)]. However, this dipole compensation seems to be incomplete in the present case, which is explained by the influence of the thick MgO spacer layer and the unusual tip position beside the particle. Furthermore, the destructive interference may be attenuated by a phase shift between driving and induced dipoles, as caused by the different dielectric properties of Ag and Mo. The visibility of horizontal plasmon modes could be facilitated by another effect. In topographic

images, the edges of Ag nanocubes display a peculiar concave shape, indicating that the tip approaches the side facets in order to maintain the preset electron current [see inset of Fig. 3(b)]. The associated reduction of the tip-sample distance temporarily enhances the optical near field and promotes excitation and radiative decay of the horizontal plasmons.

In the last part of this paper, we want to address the visibility of (1,0) and (1,1) particle plasmons as a function of bias voltage. Apparently, an excitation bias of 6.5 V is sufficient to stimulate both modes at the particle edge, but too small to excite the higher mode at the top position [Fig. 3(a)]. This observation is surprising, as the energy of exciting electrons largely exceeds the plasmon energy of 2.75 eV. It can be explained, however, when taking into account the double-barrier nature of the STM junction. In fact, the maximum energy that can be transferred from a tunneling electron is given by the voltage drop U either across the vacuum or the oxide barrier.[30] The ratio between these potential steps depends on the width d and dielectric constant ϵ of both barriers, according to $\frac{U_{\mathrm{vac}}}{U_{\mathrm{ox}}} = \frac{d_{\mathrm{vac}}/\varepsilon_{\mathrm{vac}}}{d_{\mathrm{ox}}/\varepsilon_{\mathrm{ox}}}$. If the tip is located directly above the particle, roughly 70% of the potential drops inside the vacuum barrier, while 30% decays in the oxide film. In reality, the potential drop across the oxide might be even larger, as the particle charges up in the tip-electric field. As a result of this division, energy losses of tunneling electrons will be much smaller than the applied bias voltage and thus insufficient to excite the high-energy (1,0) mode.[18] In contrast, almost the whole potential drops across the vacuum if the particle is in a side-on geometry with respect to the tip and not exposed to the full electric field any more [Fig. 4(b)]. In this configuration, sufficiently large inelastic losses are possible in the vacuum barrier to excite in-plane as well as out-of-plane plasmon modes even at 6.5 V (Fig. 3). The visibility of particle plasmons therefore depends on both the inclination of the exciting electron beam and the exact potential course in the double-barrier STM junction.

IV. CONCLUSIONS

The optical properties of individual Ag particles on an MgO(001) support have been investigated by analyzing the light-emission induced by electron injection from an STM tip. Photon maps of the cubelike Ag particles display two regions of enhanced emission, located at the edges and the center of each deposit. In the former position mainly in-plane plasmons are excited by the tip electrons, while out-of-plane modes become detectable in the latter one. This assignment is supported by the spectroscopic data, which show a broad emission band at 2.1 eV at the particle edges and a blueshifted mode at 2.7 eV at the top facet. The visibility of in-plane plasmons is a somewhat pathological effect, owing to the unusually high aspect ratio of MgO-supported Ag deposits and the possibility of generating a horizontal tunneling path into the sample. In the more general case of vertical tunneling, the out-of-plane modes always dominate the optical response due to the strong field enhancement along the tip-sample axis.

ACKNOWLEDGMENTS

We are grateful to S. Benedetti for many stimulating discussions and acknowledge support from the COST action D41.

*nilius@fhi-berlin.mpg.de.

[1] E. Abbe, Arch. Mikrosk. Anat. **9**, 413 (1873).
[2] J. G. White, W. B. Amos, and M. Fordham, J. Cell Biol. **105**, 41 (1987).
[3] M. Dyba and S. W. Hell, Phys. Rev. Lett. **88**, 163901 (2002).
[4] E. A. Ash and G. Nichols, Nature **237**, 510 (1972)
[5] J. H. Coombs, J. K. Gimzewski, B. Reihl, J. K. Sass, and R. R. Schlittler, J. Microscopy **152**, 325 (1988).
[6] R. Berndt, in *Scanning Probe Microscopy*, edited by R. Wiesendanger, Springer Series Nanoscience and Technology (Springer, Berlin, 1998), p. 97.
[7] A. Downes and M. E. Welland, Appl. Phys. Lett. **72**, 2671 (1998).
[8] N. Nilius, N. Ernst, and H.-J. Freund, Phys. Rev. Lett. **84**, 3994 (2000).
[9] S. F. Alvarado, P. Renaud, D. L. Abraham, and H. P. Meier, J. Vac. Sci. Technol. B **9**, 409 (1991).
[10] U. Hakanson, M. K. Johansson, M. Holm, C. Pryor, L. Samuelson, and W. Seifert, Appl. Phys. Lett. **81**, 4443 (2002).
[11] X. H. Qui, G. V. Nazin, and W. Ho, Science **299**, 542 (2003).
[12] E. Cavar, M.-C. Blüm, M. Pivetta, F. Patthey, M. Chergui, and W. D. Schneider, Phys. Rev. Lett. **95**, 196102 (2005).
[13] G. Schull, M. Becker, and R. Berndt, Phys. Rev. Lett. **101**, 136801 (2008).
[14] A. O. Gusev, A. Taleb, F. Silly, F. Charra, and M. P. Pileni, Adv. Mater. **12**, 1583 (2000).
[15] A. Downes and P. Dumas, Appl. Surf. Sci. **212**, 770 (2003).
[16] K. Watanabe, D. Menzel, N. Nilius, and H.-J. Freund, Chem. Rev. **106**, 4301 (2006).
[17] U. Kreibig and W. Vollmer, *Optical Properties of Metal Clusters*, Springer Series Materials Science (Springer, Berlin, 1995), Vol. 25.
[18] P. Myrach, N. Nilius, and H.-J. Freund, J. Phys. Chem. C **113**, 18740 (2009).
[19] N. Nilius, N. Ernst, and H.-J. Freund, Surf. Sci. **478**, L327 (2001); Chem. Phys. Lett. **349**, 351 (2001).
[20] S. Benedetti, H. M. Benia, N. Nilius, S. Valeri, and H.-J. Freund, Chem. Phys. Lett. **430**, 330 (2006).
[21] A. Ouahab, C. Mottet, and J. Goniakowski, Phys. Rev. B **72**, 035421 (2005).
[22] S. Schintke, S. Messerli, M. Pivetta, F. Patthey, L. Libioulle, M. Stengel, A. De Vita, and W. D. Schneider, Phys. Rev. Lett. **87**, 276801 (2001).
[23] S. Sicolo, L. Giordano, and G. Pacchioni, J. Phys. Chem. C **113**, 16694 (2009).
[24] H. M. Benia, P. Myrach, and N. Nilius, New J. Phys. **10**, 013010 (2008).

[25]We tentatively assign the fine structure to Coulomb charging effects that modulate the elastic as well as inelastic electron current through the particle sandwiched between two barriers. In particular, inelastic transitions that are responsible for light emission are only possible if the electron after excitation has the right energy to enter the particle electronic system. The charging energy for a 4-nm Ag sphere is estimated with 80 meV using the spherical capacitor model, which is in reasonable agreement with the 100-meV peak separation observed in the experiment.

[26]T. Wenzel, J. Bosbach, F. Stietz, and F. Träger, Surf. Sci. **432**, 257 (1999).

[27]R. Lazzari and I. Simonsen, Thin Solid Films **419**, 124 (2002); D. Bedeaux and J. Vlieger, *ibid.* **69**, 107 (1980).

[28]E. D. Palik (Hrsg.), *Handbook of Optical Constants of Solids* (Academic, Orlando, 1985).

[29]P. Johansson, R. Monreal, and P. Apell, Phys. Rev. B **42**, 9210 (1990).

[30]S. W. Wu, G. V. Nazin, X. Chen, X. H. Qiu, and W. Ho, Phys. Rev. Lett. **93**, 236802 (2004).